Imaging of a Surface Alloy with Energy-Dependent Photoelectron Holography

J. G. Tobin and G. D. Waddill
Chemistry and Materials Science Department, Lawrence Livermore National Laboratory, Livermore, California 94550

Hua Li and S. Y. Tong
Laboratory for Surface Studies and Department of Physics, University of Wisconsin-Milwaukee, Milwaukee, Wisconsin 53201
(Received 11 January 1993)

Fourier transformation of experimental energy-dependent photoelectron diffraction data has been used to produce an essentially artifact-free image of a surface alloy. This direct method, based upon the intersection off contour arcs associated with each measurement direction, can provide vectorial atomic positions with atomic resolution. A rapid data collection mode was introduced. Surface structural sensitivity was confirmed by comparison with multiple-scattering simulations. The previously ambiguous surface geometry of $c(2\times2)$Au/Cu(001) has been determined, with clear, non-model-dependent discrimination of the surface alloy over the overlayer structure.

PACS numbers: 79.60.Dp, 61.10.Lx, 61.14.Dc

An elusive goal of surface crystallography is the development of a reliable direct method which reveals surface geometry with atomic resolution and chemical selectivity. An interesting idea, originally proposed by Szoke [1] and extended by Barton [2], was to apply a Fourier transformation to Auger or photoelectron diffraction intensities over a wide angular range at a fixed kinetic energy. Early experimental work [3] seemed to confirm the validity of this approach. More recent investigations, based on simulated [4,5] and measured [6,7] diffraction spectra, have pointed out severe limitations of the single-energy transformation [8,9]. These limitations are due to the presence of artifacts in the reconstructed image in the form of bright spots or streaks at nonatomic positions. While simplified procedures [10] requiring more explicit prior knowledge of the structure have been suggested, the most promising method of resolution improvement, twin image suppression, and artifact removal in electron holography appears to be the utilization of multiple energies [4,11,12]. It is this necessity of using multiple energies that leads us to consider a variant of photoelectron imaging in which sampling over a wide energy range is utilized.

In this Letter we present a combined experimental and computational study that demonstrates direct wave-front reconstruction to obtain surface structure with atomic resolution using spatially resolved imaging of energy-dependent photoelectron diffraction (SRI-EDPD). The theory behind this method has been presented earlier [13], but this is the first experimental investigation utilizing this particular approach. Moreover, while Fourier transformation of experimental data provides a *direct* image of the surface structure, detailed multiple-scattering simulations and transformation of calculated intensities are used to verify the analysis. The crucial results for the $c(2\times2)$Au/Cu(001) [14–18] are shown in Fig. 1. The first in-plane nearest neighbors (Cu) and second and third in-plane nearest neighbors (Au) are imaged with atomic resolution, *without the intrusion of artifact peaks.* Such a non-model-dependent discrimination of a surface alloy from an overlayer is impossible using more-conventional diffraction techniques.

Although multiple-energy wave-front reconstruction had been carried out using experimental data [19,20], the previous works were done on bulk emission systems in which the structural information was averaged over many layers (i.e., the surface and bulk interlayer spacings mixed together). The present study is the first experimental demonstration of data inversion in which single-layer information is obtained. Because this system contains strongly scattering Au and Cu potentials, multiple wave-number phase locking is essential to the success of the reconstruction process.

While this is the first demonstration of SRI-EDPD, structural studies with energy-dependent photoelectron diffraction have been done for quite some time [21,22]. Fourier transformation of the data has also been pursued: Early works [23–27] showed that there was some validity to this method for determining *scalar* distances. The present approach involves inverting energy variation curves at a large number of angular positions and the idea is to extract *vector* (i.e., direction and distance) information relating an emitter and its neighbors.

The experiments were performed at the Stanford Synchrotron Radiation Laboratory using beam line 8-2. This is a spherical grating monochromator beam line [28,29] which is part of the UC/National Laboratories Participating Research Team (PRT) facilities. EDPD curves were collected at 48 different angular positions in the irreducible $\pi/4$ solid angle between the (010) plane and $(1\bar{1}0)$ plane of Cu(001), as illustrated in Fig. 2. The relationship between the electron collection and x-ray vectors (Poynting and linear polarization) was fixed, so as to eliminate other asymmetry contributions, the so-called β effects [30]. The electron collection cone [16] was centered parallel to the x-ray polarization. The sample nor-

0031-9007/93/70(26)/4150(4)$06.00

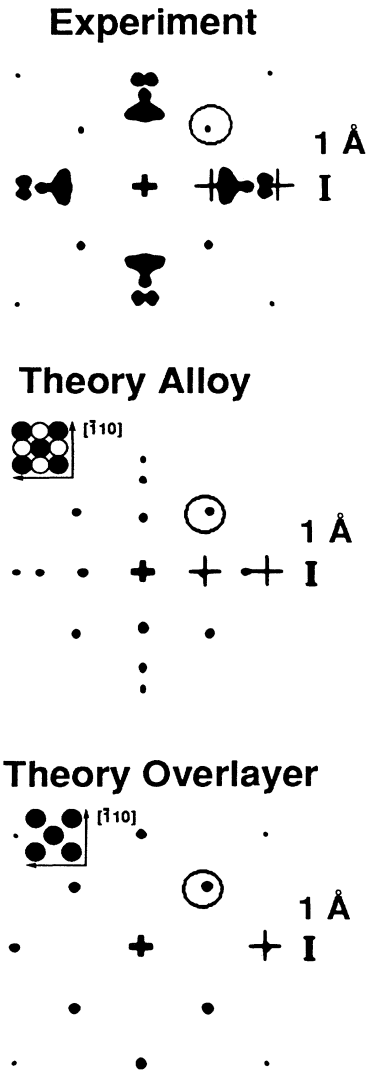

FIG. 1. Images reconstructed from experimental spectra (top), and calculated spectra from the surface alloy model (middle) and overlayer model (bottom). In each picture, the thick cross marks the Au emitter's position; thin crosses and the circle mark the expected atom positions of neighbors in a $\pi/4$ sector. The plane of view passes through the nuclei of surface layer atoms; see insets for surface models. (Au=solid circle and Cu=hollow circle.) The experiment clearly agrees with the surface alloy model.

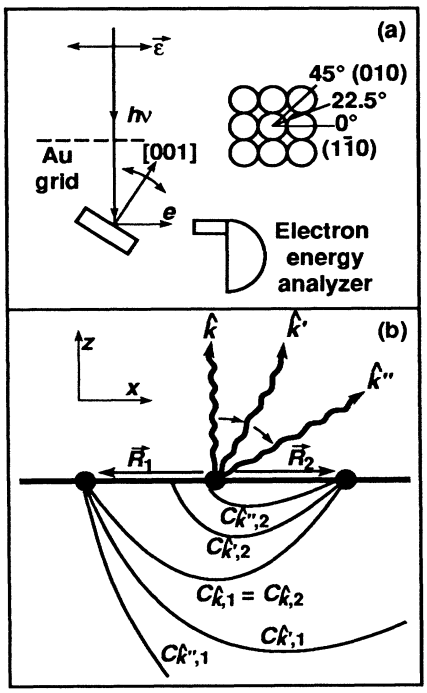

FIG. 2. (a) The geometry of the data collection and (b) single-scattering contour arcs. ε is the photon electric vector, and e is an injected electron. In (b), the intersections of the contour arcs correspond to atoms placed at ± 2 Å along the x axis, relative to the emitting atom at the origin. The contours are due to emission directions $\hat{k}$ (0°), $\hat{k}'$ (30°), and $\hat{k}''$ (60°). The z axis has been expanded by a factor of 2 relative to the x axis.

mal, the x-ray Poynting and polarization vectors, and the center of the collection cone were all approximately coplanar. Because of $\mathbf{A}\cdot\mathbf{P}$ effects [30], this configuration has a general tendency to optimize photoelectron intensities. Polar angular variation was achieved by rotating the sample, with the sample normal remaining in the plane containing the x-ray vectors and the electron collection. Azimuthal angular selection was performed by rotating the sample about the sample normal. In this case three azimuths, at 0°, 22.5°, and 45°, were used, as illustrated in Fig. 2. For each azimuthal setting, sixteen polar angles were sampled, ranging in 5° steps from 10° to 85° from normal emission. Angular alignment was performed using both LEED and laser reflection. Photon flux was measured by monitoring the photoyield of a 90% transmitting gold grid, placed upstream from the sample but after the final x-ray refocusing optics. The data were collected in a constant-initial-state (CIS) mode, as shown in Fig. 3. In previous EDPD studies, an energy distribution curve was taken at each photon energy. The area of the core peak would be determined by fitting the spectra, and oscillations in the cross section of 25% to 50% would be observed due to photoelectron diffraction [22,24–27]. To accelerate the data collection, we have utilized a fast data taking method built upon a CIS data collection mode [31] with normalization to the incident photon flux provided by the output of the Au grid, which serves as an I_0 monitor. All electrons in an energy window of 10 eV were integrated, centered upon the Au $4f_{7/2}$ and Au $4f_{5/2}$ peaks, and the integration included all electrons in the core-level peaks plus the underlying background. The photon energy was moved in 2 eV steps from $\sim$330 to 530 eV and the kinetic energy was similarly stepped from $\sim$240 to 440 eV. This allowed operation at the maxima

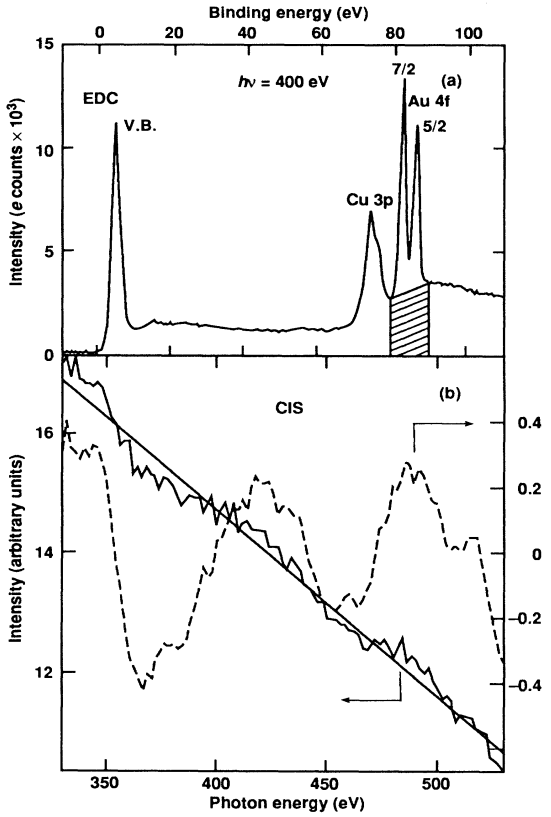

FIG. 3. Experimental data: (a) An energy distribution curve (EDC) collected at a photon energy of 400 eV. (b) A CIS spectrum taken in the 45° azimuth at a polar angle of 70°. Both normalized (solid) and subtracted (dashed, expanded) curves are shown. The expanded data curve includes the effect of a five-point smoothing procedure.

of the Au $4f$ cross section and of the output of the gold grid I_0 monitor [28,29,31]. Using a Au grid as the I_0 monitor had an additional advantage: At these photon energies the Au photoyield should be dominated by the Au $4f$ contribution [31,32]. Division of the analyzer output by the Au photoyield thus not only provided a normalization to photon flux but also removed in large part the atomic Au $4f$ contribution to cross-section variations. (The result of this cancellation is the acceptability of using a linear background function, discussed below. In the usual case, where the grid materials and sample are different, a more general function, such as a spline, could be used to accommodate the cross-section effects of both the sample and grid materials, following the example of extended x-ray-absorption fine-structure spectroscopy studies and previous photoelectron diffraction experiments.)

A typical CIS curve for a single angle is shown in Fig. 3. The normalized data with a least-squares linear fit and the subtracted data are both shown. The overall decreasing magnitude of the normalized CIS data (Fig. 3) arises because of the following: As the photon energy increases, the kinetic energy also increases and the analyzer transmission is inversely proportionate to kinetic energy [31]. This monotonic variation can be approximately removed by fitting each EDPD curve to a straight line, which is then subtracted to isolate the EDPD cross-section modulations. Because the oscillations have long wavelengths in energy space (~75 eV) and the window width was fairly wide (~10 eV), data smoothing was utilized to decrease discontinuities between individual 2 eV channels. The oscillations thus determined are only about 3%, down an order of magnitude from the 25%–50% effects found using the peak fitting procedures [22,24–27]. Nevertheless, the oscillations are easily observable. Moreover, the rate of data collection has improved by at least an order of magnitude, thus permitting the taking of a total set (3 azimuths, 16 polar angles, 200 eV wide scans with 2 eV steps) with a total data acquisition time of about 12 h. The resulting $\pi/4$ solid angle has about 5000 points in momentum space, which is a fairly dense grid. Additional control experiments were run to collect the same CIS curves using clean Cu(001) as the sample. Such control experiments confirmed that the Cu $3p$ photoemission was not the cause of the observed modulation. The results of the control experiment will be published elsewhere. Prior to data inversion, all the EDPD oscillation curves were normalized versus $h\nu$ and then to each other, the latter to eliminate any spurious intensity variations associated with luminosity or electron optics, for example, due to the variation of sample position.

Analysis of the experimental EDPD curves followed the procedure set forth in the work of Tong *et al.* [13]. At these kinetic energies, artifacts from multiple scattering can be quite strong. However, using EDPD curves at a variety of angles eliminates the multiple scattering artifacts. This is because Fourier transformation of EDPD curves produces contour arcs, associated with single- and multiple-scattering path lengths. The single scattering arcs for all EDPD curves intersect at atomic positions [13], producing an amplitude peak scaling as N, the number of EDPD curves (Fig. 2). The multiple-scattering contour arcs, on the other hand, intersect only two at a time, and these intersections spread diffusely over real space. Because intensity is equal to the amplitude squared, the intensities of the single-scattering arc intersections (at atomic positions) tend to increase over multiple-scattering intersections (at artifacts) by a ratio of $(N/2)^2$. Hence, with 48 EDPD curves as in our case, ideally the single-scattering to multiple-scattering ratio should be $(24)^2$ or 576. Because of the finite energy range of the EDPD curves, which broadens the contour arcs in real space, and the tendency for multiple-scattering contour intersections to occur near to each other, the actual ratio is not as large as the ideal case. Nevertheless, sufficient reduction of multiple-scattering effects occurs to eliminate any artifacts inside the first

two nearest neighbor shells, as illustrated in Fig. 1. On a scale of 1 to 105, along the [110] direction, the image of the nearest neighbor atom (Cu) has an intensity of 103, and the third neighbor atom (Au) has an intensity of 73. Along the [100] direction, the second neighbor atom (Au) has an intensity of 60 and the fifth neighbor atom has an intensity of 6. All artifacts have intensities below 5. Although some peak distortion and shifting relative to the true positions can be observed in Fig. 1, all of this is easily within 1 Å. This observation can be discussed more effectively by comparison to the simulation of theoretical spectra.

Also shown in Fig. 1 are two Fourier transformations (FT) of calculated EDPD curves, generated by applying multiple scattering theory to the $c(2\times2)$Au/Cu(001) surface alloy and overlayer models. Even in images obtained from the theoretical curves, some peak position shifting occurs. The shifts are due to anisotropic factors (both in phase and magnitude) of the Au and Cu scattering factors [33]. The salient result in Fig. 1 is that the FT of both the surface alloy and overlayer simulations recover the essence of each real space model, without the addition of artifact peaks. However, it appears that peak position shifting becomes progressively worse moving away from the central emitter. Thus only first and second nearest neighbor positions can be determined accurately with this database. (The data ranges used in the theoretical and experimental inversions are identical.) In the case of the overlayer, a less areally dense structure, the second nearest neighbors are 5.1 Å away, but in the surface alloy these atoms are now third nearest neighbors and exhibit greater shifting as well as peak splitting. Splitting of outer shell atomic images, due to shadowing by an inner shell atom and multiple scattering, has been observed previously in simulations [13]. The lateral distortion of the nearest neighbor Cu peaks in the experimental FT is absent in the surface alloy simulation: This appears to be related to surface vibrations in the real sample as well as systematic uncertainties in the data acquisition, such as sample alignment, and the limited size of the data set.

In summary, the reconstruction formula for inverting EDPD spectra has been applied to experimental data. First results for the $c(2\times2)$Au/Cu(001) system are encouraging, demonstrating two-dimensional vectorial imaging. By achieving atomic resolution of less than 1 Å, the reconstruction image shows directly and conclusively that the Au/Cu(001) system involves alloying in the surface layer.

This work was conducted in part under the auspices of the U.S. Department of Energy by LLNL under Contract No. W-7405-ENG-48. The SSRL is supported by DOE/BES. The work at the University of Wisconsin-Milwaukee was supported by NSF Grant No. DMR-9214054. Karen Clark provided clerical support for this work at LLNL.

[1] A. Szoke, in *Short Wavelength Coherent Radiation Generation and Applications,* edited by D. T. Attwood and J. Boker, AIP Conf. Proc. No. 142 (American Institute of Physics, New York, 1986).
[2] J. J. Barton, Phys. Rev. Lett. **61**, 1356 (1988).
[3] G. K. Harp *et al.*, Phys. Rev. Lett. **65**, 1012 (1990).
[4] H. Huang *et al.*, Phys. Rev. B **44**, 3240 (1991).
[5] S. Thevuthasan *et al.*, Phys. Rev. Lett. **67**, 469 (1991).
[6] S. A. Chambers *et al.*, J. Vac. Sci. Technol. B **10**, 2092 (1992).
[7] A. Stuck *et al.*, Surf. Sci. **264**, 380 (1992); **274**, 441 (1992).
[8] L. J. Terminello and J. J. Barton, Science **251**, 1218 (1991).
[9] S. A. Chambers, Adv. Phys. **40**, 357 (1991), and references therein; Surf. Sci. Rep. **16**, 261 (1992), and references therein.
[10] R. Dippel *et al.*, Phys. Rev. Lett. **68**, 1543 (1992).
[11] J. J. Barton and L. J. Terminello, in *The Structure of Surfaces-III,* edited by S. Y. Tong, M. A. Van Hove, X. Xie, and J. Takayanagi (Springer, Berlin, 1991); J. J. Barton, Phys. Rev. Lett. **67**, 3106 (1991).
[12] S. Y. Tong *et al.*, Phys. Rev. Lett. **67**, 3102 (1991).
[13] S. Y. Tong *et al.*, Phys. Rev. B **46**, 2452 (1992).
[14] P. W. Palmberg and T. N. Rhodin, J. Chem. Phys. **49**, 134 (1968); **49**, 147 (1968).
[15] Z. Q. Wang *et al.*, Solid State Commun. **62**, 181 (1987).
[16] J. G. Tobin *et al.*, J. Vac. Sci. Technol. A **8**, 2494 (1990), and references therein.
[17] D. Naumovic *et al.*, Surf. Sci. **269/270**, 719 (1992); Surf. Sci. (to be published).
[18] D. D. Chambliss *et al.*, J. Vac. Sci. Technol. A **10**, 1993 (1992).
[19] L. J. Terminello *et al.*, J. Vac. Sci. Technol. B **10**, 2088 (1992).
[20] H. Li *et al.*, Phys. Rev. B **47**, 10036 (1993).
[21] S. Y. Tong and C. H. Li, Bull. Am. Phys. Soc. **23**, 417 (1978); C. H. Li and S. Y. Tong, Phys. Rev. B **19**, 1769 (1979); Phys. Rev. Lett. **42**, 901 (1979); **43**, 526 (1979).
[22] S. D. Kevan *et al.*, Phys. Rev. Lett. **41**, 1565 (1978).
[23] Z. Hussain *et al.*, Proc. Natl. Acad. Sci. U.S.A. **78**, 5293 (1981).
[24] D. H. Rosenblatt *et al.*, Phys. Rev. B **23**, 3828 (1981).
[25] J. G. Tobin *et al.*, Phys. Rev. B **26**, 7076 (1982); S. Y. Tong *et al.*, Phys. Rev. B **27**, 4632 (1983).
[26] J. J. Barton *et al.*, Phys. Rev. Lett. **51**, 272 (1983).
[27] C. C. Bahr *et al.*, Phys. Rev. B **35**, 3773 (1987).
[28] K. G. Tersell and V. P. Karpenko, Nucl. Instrum. Methods Phys. Res., Sect. A **291**, 511 (1990).
[29] L. J. Terminello *et al.*, Nucl. Instrum. Methods Phys. Res., Sect. A **319**, 271 (1992).
[30] R. F. Davis *et al.*, Chem. Phys. Lett. **71**, 448 (1980).
[31] J. G. Tobin *et al.*, Symp. Proc. Mat. Res. Soc. (to be published).
[32] J. J. Yeh and I. Lindau, At. Data Nucl. Data Tables **32**, 1 (1985).
[33] S. Y. Tong *et al.*, Phys. Rev. Lett. **66**, 60 (1991).